Chemical Softness as a Predictor for Reactivity at Metal Surfaces

Amy L. Gunton and Stephen J. Jenkins
Yusuf Hamied Department of Chemistry, University of Cambridge, Lensfield Road, Cambridge CB2 1EW, United Kingdom
(Dated: December 19, 2025)

LITERATURE REVIEW OF EXPERIMENTALLY DETERMINED CO ADSORPTION SITES

In order to choose which geometry and coverage to use for CO adsorption calculations, a review was conducted of the experimental literature. The results are summarised in Table S1.

Table S1 summarises the experimental literature reports on the structure of the surfaces, both with and without a CO overlayer. Figure S1 illustrates the geometry at which CO was assumed to adsorb in this study. For most cases, there was consensus in the literature about the structures, but for some surfaces there was less agreement.[1]

There is some uncertainty about the adsorption site for CO on Rh{110}.[1] While it is known that CO adsorbs on the short bridge site with a p2mg (2×1) structure at 1 ML coverage, there is little consensus in the literature about whether CO adsorbs at the same site or atop in the 0.5 ML coverage c(2×2) structure.[1,3] An early study by Marbrow and Lambert[2] found that the temperature programmed desorption (TPD) spectra had a single peak. They suggested from this that the adsorption site at 0.5 ML must match that for 1 ML. As Batteas[3] and others[1] found that the adsorption site for 1 ML of CO on Rh{110} is the short bridge, this suggests that the 0.5 ML adsorption site must be the same. However, Dhanak and co-workers[20] performed an X-ray photoelectron spectroscopy (XPS) study that suggested that CO adsorbs atop at 0.5 ML and transitions to the short bridge site at higher coverages. Wei and co-workers[1] made a thorough review of the literature prior to 1997 and said that while no firm conclusion could be made, the evidence better supported the short bridge site at 0.5 ML.

CO adsorbs on the Pd{110} surface to form an ordered overlayer with a distinctive LEED pattern indicating a (2×1) cell with p2mg symmetry.[1] The glide symmetry arises from CO having alternating tilts along the close-packed rows. The Pt{110} surface exhibits a missing row reconstruction under UHV conditions, which is lifted in the presence of CO.[9] Comrie and Lambert[9] found that this overlayer was analogous to that formed on Pd{110}.

There are not many literature reports on CO adsorption on gold and silver and what reports there are often disagree.[14,21] The adsorption heat is small, and for some surfaces there may be no ordered overlayer.[11] Interestingly, the adsorption heat for CO on silver was found by several studies to be lower than that for gold, in contradiction to conventional wisdom regarding the relative reactivities of these metals, but corresponding to the lower atomic softness for silver compared with gold which was found in the current study.[21] For the purposes of this work we have assumed CO adsorbs on the {111}, {100} and {110} gold and silver surfaces in an ordered overlayer. We have further assumed that this ordered overlayer has the same structure as the overlayer of CO on the equivalent copper surface. These assumptions are illustrated in Fig. S1.

Concerning adsorption of CO on the Au{110} surface, some studies suggest an ordered CO overlayer and a lifting of the reconstruction, whereas others differed.[15,22] One study, by Gottfried and co-workers[23], found no long-range order to the CO overlayer on Au{110}. They also did some angle-resolved ultra-violet photoemission spectroscopy (ARUPS) measurements that suggested that CO may adsorb parallel to the surface. Meyer et al[22] report that for a wide range of temperatures and pressures of CO the reconstruction was not lifted. In contrast to these findings, Jugnet et al[19] suggest that CO lifts the reconstruction to result in a (1×1) cell. The same authors thought that CO linearly chemisorbs in an atop position.[19] However, it should be noted that just because the reconstruction was lifted to form a (1×1) cell in the presence of CO, that does not necessarily mean that an ordered overlayer of CO formed with (1×1) symmetry.[9] LEED is a diffraction technique and therefore only shows ordered surface structure. A disordered overlayer would therefore be invisible to LEED, other than contributing to a diffuse background.

In a similar case to Au{110}, early studies of Au{100} found no ordered CO overlayer.[22] However, later studies by Pierce and co-workers have found that at higher pressures of CO there is a stable overlayer formed.[15,17] The same authors also found that CO adsorption lifted the hexagonal reconstruction of Au{100} to a (1×1) structure.[17] Pierce et al[17] did not report an adsorption site for CO on Au{100}, but Nakamura and co-workers[18] found that their polarization modulation infrared reflection absorption spectroscopy (PM-IRAS) results were consistent with CO adsorbing atop Au atoms.

Similarly, for Au{111}, early studies found that adsorption of CO lifted the herringbone $(23 \times \sqrt{3})$ reconstruction and (under certain conditions of high temperature and CO pressure) restored the (1×1) structure.[22,24] However, they also found that the surface might not form an ordered (1×1) overlayer.[22,24] In contrast, while later authors agreed with Peters et al in finding that CO lifted the herringbone reconstruction, they also found that the reconstruction was completely lifted at 250 Torr, resulting in a (1×1) structure, with CO adsorbed atop.[16] For the purposes of this work we have assumed that CO forms an ordered overlayer on Au{111} that has the same structure as that formed by CO on Cu{111}.

In terms of CO adsorption on Ag{111}, Abild-Pedersen and co-workers report that CO adsorbs atop.[10] However, other literature reports suggest that there is no ordered overlayer for CO on Ag{111}.[11,12] Work by Hansen and co-workers[12] suggests the CO molecules have a random orientation on Ag{111}. For the Ag{110} surface, the literature

Surface	Clean structure	Adsorption site	Adsorption structure	θ/ ML	References
Rh{111}	(1×1)	atop	$(\sqrt{3} \times \sqrt{3})$ R30°	1/3	[1]
Rh{100}	(1×1)	atop	$c(2 \times 2)$	1/2	[1–3]
Rh{110}	(1×1)	short bridge	$c(2 \times 2)$	1/2	[1]
Pd{111}	(1×1)	fcc hollow	$(\sqrt{3} \times \sqrt{3})$ R30°	1/3	[1]
Pd{100}	(1×1)	bridge	$(2\sqrt{2} \times \sqrt{2})$ R45°	1/2	[1, 4, 5]
Pd{110}	(1×1)	atop	(2×1)	1 $*$	[1, 6]
Pt{111}	(1×1)	atop	$(\sqrt{3} \times \sqrt{3})$ R30°	1/3	[1]
Pt{100}	hexagonal	atop	$c(2 \times 2)$	1/2	[7, 8]
Pt{110}	(1×2)	atop	(2×1)	1	[9]
Cu{111}	(1×1)	atop	$(\sqrt{3} \times \sqrt{3})$ R30°	1/3	[1]
Cu{100}	(1×1)	atop	$c(2 \times 2)$	1/2	[1]
Cu{110}	(1×1)	atop	(2×1)	1/2	[1]
Ag{111}	(1×1)	atop			[10–12]
Ag{100}	(1×1)				[13]
Ag{110}	(1×1)				[14]
Au{111}	$(23 \times \sqrt{3})$	atop	(1×1)	†	[15, 16]
Au{100}	hexagonal	atop	(1×1)	†	[15, 17, 18]
Au{110}	(1×2)	atop	(1×1)	†	[15, 19]

TABLE S1: Table showing the geometry of metal surfaces with and without CO adsorbed. Where the clean surfaces exhibited a reconstruction, the coverage of CO was chosen such as lifted the reconstruction, for example for Au{111} and Au{110}. The results for all three facets of Rh, Cu and Pd as well as the {111} facet of Pt were taken from Table 2 in an article by Wei and co-workers.[1] $*$ = The Pd{110}-CO system exhibits a reconstruction between coverages of 0.3-0.75 ML.[1,6] †= For these surfaces we could not find a definitive literature reference for the coverage or adsorption structure. The cited references state that the reconstruction was lifted with CO adsorption to form a (1×1) LEED pattern, but this does not mean that there was necessarily an ordered CO overlayer with (1×1) periodicity. There may have been a disordered layer of CO that would not be evident in the LEED pattern.

suggests the CO is very weakly bound, and may even be bound with a random orientation, or with the CO bond parallel to the surface.[14] There has been little reported in the literature on the adsorption of CO on a clean Ag{100} surface. However, work by Burghaus and co-workers[13] suggests that the clean surface does not reconstruct.

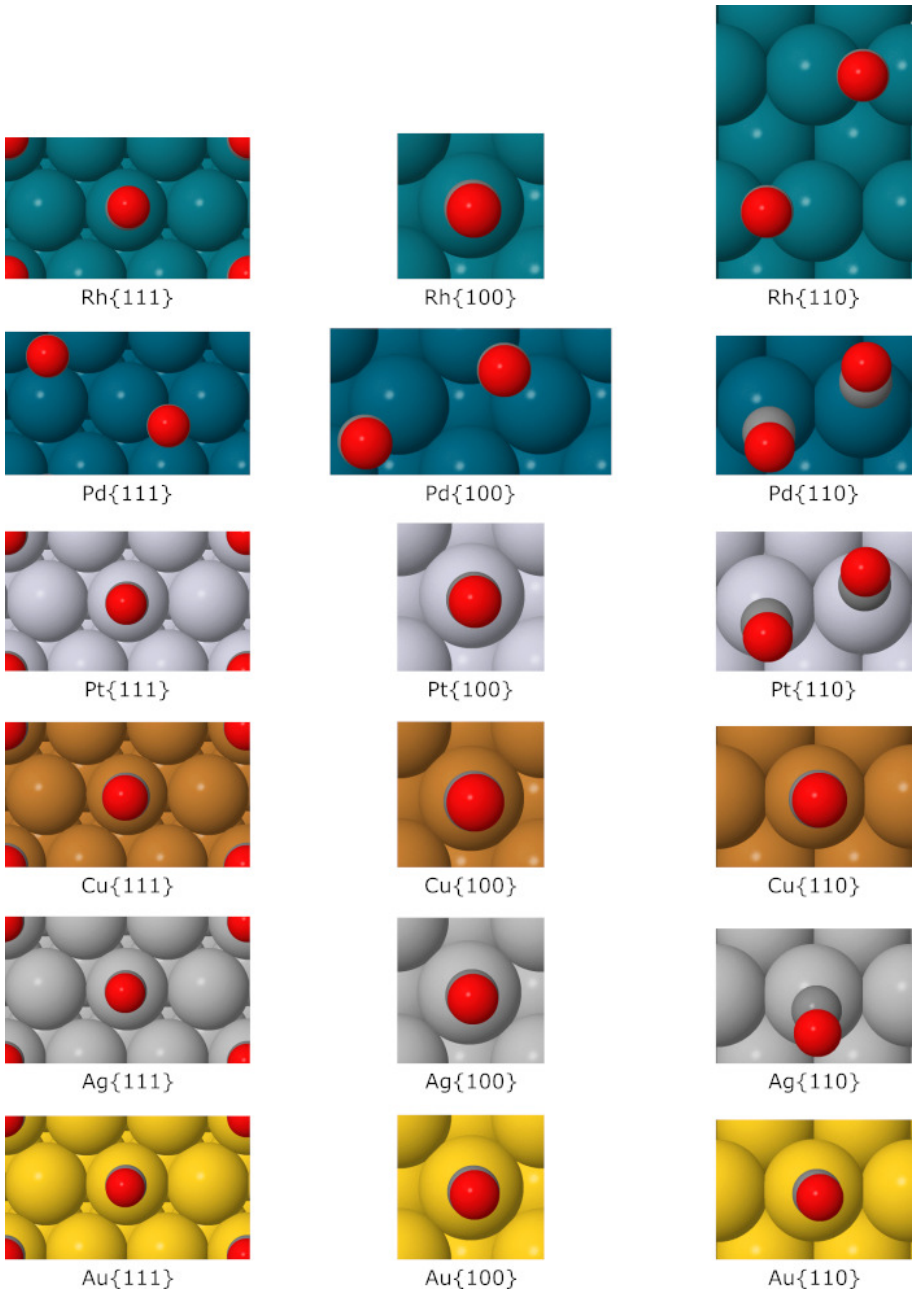

Figure S1: Figures showing the optimised CO adsorption sites starting from the literature lowest-energy adsorption positions.

GEOMETRIES USED FOR CALCULATIONS WITH CO IN ATOP SITE AT LOW COVERAGE

The following cell sizes and Brillouin-zone sampling meshes were used for calculations of adsorption heat at low CO coverage in the atop site.

Surface	Adsorption structure	θ/ ML	**k**-points
Rh{111}	$(\sqrt{3} \times \sqrt{3})$ R30°	1/3	$8 \times 8 \times 1$
Rh{100}	c(2×2)	1/2	$6 \times 6 \times 1$
Rh{110}	c(2×2)	1/2	$5 \times 5 \times 1$
Pd{111}	$(\sqrt{3} \times \sqrt{3})$ R30°	1/3	$5 \times 5 \times 1$
Pd{100}	$(2\sqrt{2} \times \sqrt{2})$ R45°	1/2	$3 \times 6 \times 1$
Pd{110}	(2×1)	1/2	$4 \times 6 \times 1$
Pt{111}	$(\sqrt{3} \times \sqrt{3})$ R30°	1/3	$8 \times 8 \times 1$
Pt{100}	c(2×2)	1/2	$6 \times 6 \times 1$
Pt{110}	(2×1)	1/2	$4 \times 6 \times 1$
Cu{111}	$(\sqrt{3} \times \sqrt{3})$ R30°	1/3	$8 \times 8 \times 1$
Cu{100}	c(2×2)	1/2	$6 \times 6 \times 1$
Cu{110}	(2×1)	1/2	$4 \times 6 \times 1$
Ag{111}	$(\sqrt{3} \times \sqrt{3})$ R30°	1/3	$8 \times 8 \times 1$
Ag{100}	c(2×2)	1/2	$6 \times 6 \times 1$
Ag{110}	(2×1)	1/2	$4 \times 6 \times 1$
Au{111}	$(\sqrt{3} \times \sqrt{3})$ R30°	1/3	$8 \times 8 \times 1$
Au{100}	c(2×2)	1/2	$6 \times 6 \times 1$
Au{110}	(2×1)	1/2	$4 \times 6 \times 1$

TABLE S2: CO adsorption geometries and Brillouin zone sampling used in each case.

SUPERCELL GEOMETRIES FOR CO ADSORPTION CALCULATIONS

Table S3 shows the supercell geometries which were used for the softness denominator calculations. n_s and n_v were used to denote the number of slab and vacuum layers respectively.

The slab thickness was calculated as

$$d_\mathrm{s} = c\frac{n_\mathrm{s}}{n_\mathrm{s} + n_\mathrm{v}} \tag{1}$$

where c is the supercell surface-normal dimension. There is a similar expression for the vacuum thickness,

$$d_\mathrm{v} = c\frac{n_\mathrm{v}}{n_\mathrm{s} + n_\mathrm{v}} \tag{2}$$

The value of c in each case was based on theoretical lattice constants, obtained by optimising primitive unit cells with convergence parameters consistent with those used in the subsequent surface calculations.

Surface	n_s	n_v	n_relax	$d_\mathrm{s}/\mathring{A}$	$d_\mathrm{v}/\mathring{A}$	$c/\mathring{A}$
Rh{111}	9	9	3	20.0	20.0	39.9
Rh{100}	10	10	3	19.2	19.2	38.4
Rh{110}	14	14	4	19.0	19.0	38.1
Pd{111}	8	8	3	18.0	18.0	36.1
Pd{100}	10	10	3	19.5	19.5	38.9
Pd{110}	14	14	4	19.3	19.3	38.5
Pt{111}	8	8	3	18.3	18.3	36.6
Pt{100}	10	10	3	19.8	19.8	39.6
Pt{110}	13	13	4	18.2	18.2	36.4
Cu{111}	9	9	3	18.7	18.7	37.4
Cu{100}	10	10	3	18.1	18.1	36.2
Cu{110}	15	15	4	19.1	19.1	38.2
Ag{111}	8	8	3	19.0	19.0	38.0
Ag{100}	9	9	3	18.5	18.5	37.0
Ag{110}	13	13	4	18.9	18.9	37.8
Au{111}	8	8	3	19.2	19.2	38.5
Au{100}	9	9	3	18.7	18.7	37.5
Au{110}	13	13	4	19.1	19.1	38.3

TABLE S3: Table showing the numbers of slab and vacuum layers, the number of layers of metal which were relaxed on each side of the slab, the thickness of slab and vacuum and the surface-normal supercell dimension c.

COMMENTS ON PBE ADSORPTION ENERGIES FOR CO ON TRANSITION METALS

As noted in the main text, the literature indicates a tendency for PBE calculations to overestimate the magnitude of adsorption energies for CO on transition metals. Here, we wish to provide some further points of comparison based upon our own present calculations for rhodium, palladium, and platinum.

The first point of difficulty when comparing theoretical and experimental adsorption energies relates to the coverage regimes probed and to the definition of adsorption energy itself. In calculations performed at a particular coverage, the usual definition of adsorption energy corresponds to the mean energy change per adsorbed molecule when building up from zero coverage to the coverage addressed in the calculations. In contrast, two of the most accurate experimental methods for determining adsorption energy – namely isosteric and microcalorimetirc techniques – provide instead the change in energy for each newly added molecule over and above the current coverage of the surface. The former quantity is often described as the integral adsorption energy (i.e. minus the integral adsorption energy) the integral adsorption heat, while the latter is the differential adsorption energy (i.e. minus the differential adsorption heat). Where a graph of differential adsorption energy is provided in the literature, it is of course possible to estimate the integral adsorption energy by averaging from zero coverage up to the desired coverage. In Table S4, this has been done with microcalorimetric data to provide integral adsorption energies for six systems – even though the papers cited provide only differential adsorption energies.

Where isosteric or microcalorimetric results are not available, we turn to adsorption energies estimated from temperature-programmed desorption experiments. Technically, these provide estimates of the desorption barrier (subject to various assumptions of varying fidelity) and thus only a ceiling for the true adsorption energy. On the other hand, since the experiments involve desorption of the entire original overlayer, they do correspond more closely to the integral concept than to the differential. We have used literature values of the low-coverage adsorption energies inferred from desorption for the 0.00 ML limit in the remaining three of our systems. In all of these cases, the magnitude of the adsorption energy drops substantially with increasing coverage, but the data provided in the literature does not permit straightforward estimation of the integral values at the coverages we have used in our calculations.

Nevertheless, the overall pattern is clear. In six of our nine transition metal systems, the PBE-calculated adsorption energy is significantly overestimated relative to the quoted experimental value (on average by 50%). In the case of Pd{110}, an apparent small underestimate is readily explained by the fact that the experimental value relates to the low-coverage limit and not to the integral adsorption energy at the coverage actually calculated. Only in the cases of Pt{100} and Pt{111} is there a true underestimation, by 3.8% and by 2.5%, respectively. Inclusion of Tkatchenko-Scheffler dispersion corrections would convert these to overestimates by 6.4% and 9.8%, respectively, and for those systems already overestimated at PBE level the discrepancy would become worse still.

Surface	Calculated/ eV	Experimental/ eV
Rh{100}	-1.998 @ 0.50 ML	-1.22 @ 0.50 ML (microcalorimetric)[25]
Rh{110}	-2.098 @ 0.50 ML	-1.35 @ 0.00 ML (thermal desorption)[2]
Rh{111}	-1.960 @ 0.33 ML	-1.37 @ 0.00 ML (thermal desorption)[26]
Pd{100}	-2.101 @ 0.50 ML	-1.40 @ 0.50 ML (microcalorimetric)[27]
Pd{110}	-1.666 @ 0.50 ML	-1.73 @ 0.00 ML (thermal desorption)[28]
Pd{111}	-2.219 @ 0.33 ML	-1.40 @ 0.33 ML (microcalorimetric)[29]
Pt{100}	-2.050 @ 0.50 ML	-2.13 @ 0.50 ML (microcalorimetric)[30]
Pt{110}	-2.201 @ 0.50 ML	-1.71 @ 0.50 ML (microcalorimetric)[31]
Pt{111}	-1.736 @ 0.33 ML	-1.78 @ 0.33 ML (microcalorimetric)[32]

TABLE S4: Table showing CO adsorption energies for nine transition metal surfaces, as calculated in this work using the PBE functional without dispersion correction. Experimental values are derived from desorption or calorimetric experiments as indicated. In the latter case, we have estimated the integral adsorption energies at the stated coverages by examination of the differential adsorption heats provided in the cited papers.

VARIATION OF APPARENT WORK FUNCTION WITH CHARGE AND VACUUM THICKNESS

We take this opportunity to discuss the effect of surface charging upon the work function of a metal. In doing so, we focus upon Pd{100} as our example, but believe that a similar picture should hold for other similar surfaces. In Fig. S2, we plot the planar-averaged electric potential as a function of distance from the slab centre, relative to the calculated Fermi level. The work function may then be obtained from the value of the potential in the middle of the vacuum region. Our estimate for the neutral case is not fully converged within the geometries studied here, but lies close to 5.06 eV (cf. 5.22 eV for polycrystalline palladium[33] according to experiment).

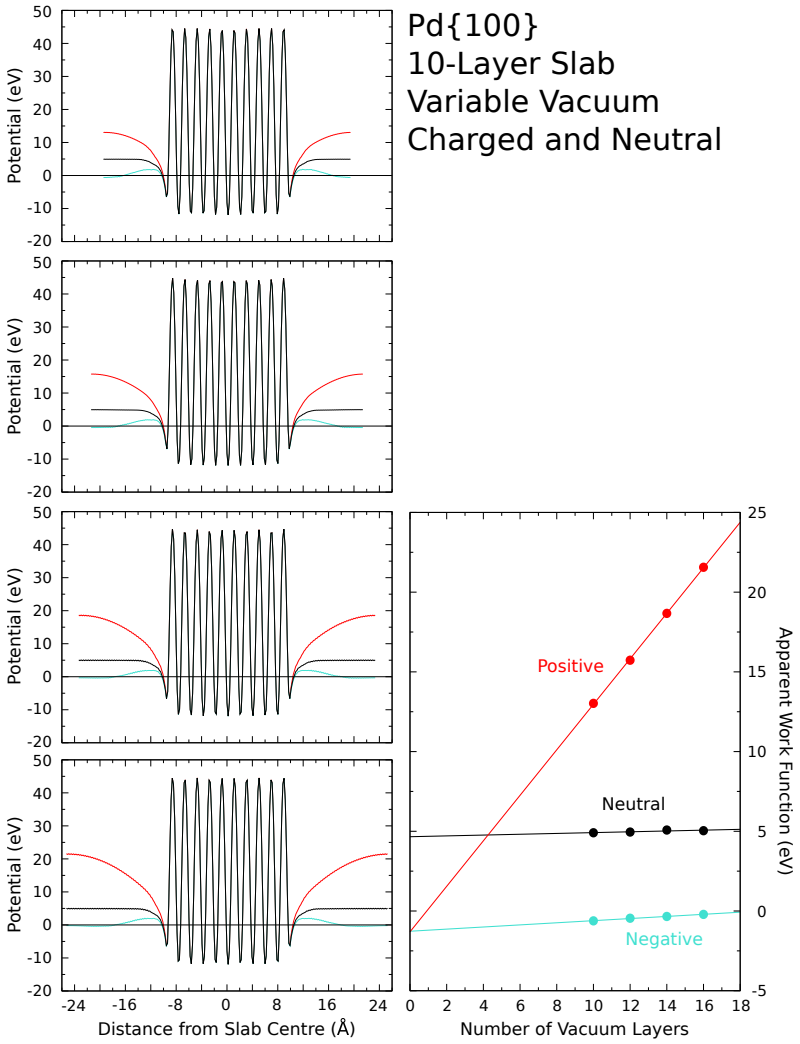

Figure S2: The left-hand panels depict the calculated electric potentials for a series of supercells of differing lengths, each containing an eight-layer Pd{100} slab. Black curves are for the neutral case, whereas red and blue curves represent cases bearing positive and negative surface excess charges respectively (± 0.02 e.Å^{-2}). The right-hand panel shows the apparent work function with respect to the number of vacuum layers (n_v) using the same colour code.

In the positively charged case, however, the apparent work function varies linearly with the thickness of the vacuum region, consistent with expectations from classical electrostatics that the potential due to an infinite charged plate should vary linearly with distance. In effect, the work function is now poorly defined. Extrapolating back to a vacuum thickness of zero yields a limiting work function of -1.31 eV, but quite what physical meaning should be attached to this is unclear. Interestingly, the apparent work functions obtained in the negatively charged case extrapolate back to almost the same value (-1.27 eV) but in all of these calculations the vacuum potential dips below zero and electron density therefore accumulates in the vacuum region; this screens the effect of the surface monopole, resulting in a very shallow gradient with respect to vacuum thickness, and indeed one that trends in the opposite direction to that which one would otherwise expect.

COMMENTS ON SPIN POLARISATION

The Slater model of itinerant ferromagnetism predicts spontaneous magnetisation when the density of states at the Fermi level of a metallic system exceeds a certain threshold – a circumstance that occurs amongst the pure elements only for iron, cobalt, and nickel. In systems where the effective coordination number is lowered, however, the d-band of other transition metals may be sufficiently narrowed – and the Fermi-level density of states concomitantly raised – as to predispose toward a ferromagnetic solution Just such a situation may be found in metallic thin films, and could even conceivably happen at native metal surface in the right circumstances. Such circumstances might include the imposition of surface excess charge, so as to shift the Fermi level up or down in energy – perhaps into an energy window where the density of states that exceeds the Stoner criterion.

In our case, although we carry out calculations with a finite surface excess charge (± 0.02 e.Å^{-2}) our intention in doing so is to estimate a gradient (i.e. the softness) in the charge-neutral limit. We believe it is most consistent, therefore, to perform our density functional calculations with spin restricted to be precisely zero. Nevertheless, we include here a brief summary of results for spin-unrestricted calculations on palladium surfaces. Given trends in valence occupancy and bandwidth as one moves horizontally and vertically within the d-block, we expect rhodium to be a little more susceptible to magnetic instability in response to surface excess charge, and platinum to be a little less. Our results for palladium are summarised in Table S5.

Surface	Negative	Neutral	Positive
Pd{100}	0.0000 μ_B (0.0000 eV)	0.0000 μ_B (0.0000 eV)	0.0000 μ_B (0.0008 eV)
	0.0233 μ_B (0.0163 eV)	0.0004 μ_B (0.0000 eV)	0.0008 μ_B (0.0008 eV)
	0.3717 μ_B (0.0082 eV)	0.0016 μ_B (0.0000 eV)	0.2702 μ_B (0.0000 eV)
Pd{110}	0.0000 μ_B (0.0005 eV)	0.0000 μ_B (0.0007 eV)	0.0000 μ_B (0.0012 eV)
	0.1537 μ_B (0.0000 eV)	0.1852 μ_B (0.0000 eV)	0.2178 μ_B (0.0000 eV)
Pd{111}	0.0000 μ_B (0.0215 eV)	0.0000 μ_B (0.0124 eV)	0.0000 μ_B (0.0145 eV)
	0.2660 μ_B (0.0189 eV)	0.1938 μ_B (0.0120 eV)	0.2469 μ_B (0.0136 eV)
	0.4954 μ_B (0.0000 eV)	0.4490 μ_B (0.0000 eV)	0.4760 μ_B (0.0000 eV)

TABLE S5: Magnetic moments and energies (both per atom) for Pd{100} as a 10-layer slab, Pd{110} as a 13-layer slab, and Pd{111} as an 8-layer slab. In each case, the top line was obtained from a strictly spin-unpolarised calculation. Other lines were obtained by relaxing the total slab spin from a starting value of either 0 μ_B or 1 μ_B. Note that magnetic moments were obtained by summing the net magnitude of the spin across a real-space grid, not the net spin itself. In all cases, the sum of the net spin (as opposed to its magnitude) was very close to zero.

As can be seen from the tabulated data, strictly unpolarised solutions are straightforwardly the most stable only for the negative and neutral Pd{100} slabs. In all other cases, solutions with spin-per-atom in the range 0.15–0.50 μ_B are more favourable, although by less than 0.0015 eV per atom for the positive Pd{100} slab and all of the Pd{110} slabs. Only for the Pd{111} slabs does the preference for spin-polarised solutions become substantial, but even here we must take note that calculations based upon ultrasoft psuedopotentials – at least for iron – can overstate the stability of high-spin solutions y as much as 0.06 eV.μ_B^{-1} relative to all-electron calculations.[34] Viewed in this light, it is not clear that the high-spin solutions found here should be given much credence. Moreover, all of the high-spin solutions were, in fact, antiferromagnetic and featured significant spin throughout the slab. That is, they were patently unphysical, implying an incorrect ferromagnetic state for bulk palladium.

In summary, we found that inclusion of spin gave rise only to unphysical solutions whose energy was lower than that of the spin-unpolarised solutions by an amount less than the likely error inherent in using ultrasoft pseudopotentials for the calculations. Given that our intention is to use our finite-charge calculations to infer results for infinitesimal charge, in which situation any spin polarisation ought to vanish anyway, we opted not to include spin polarisation in our production calculations.

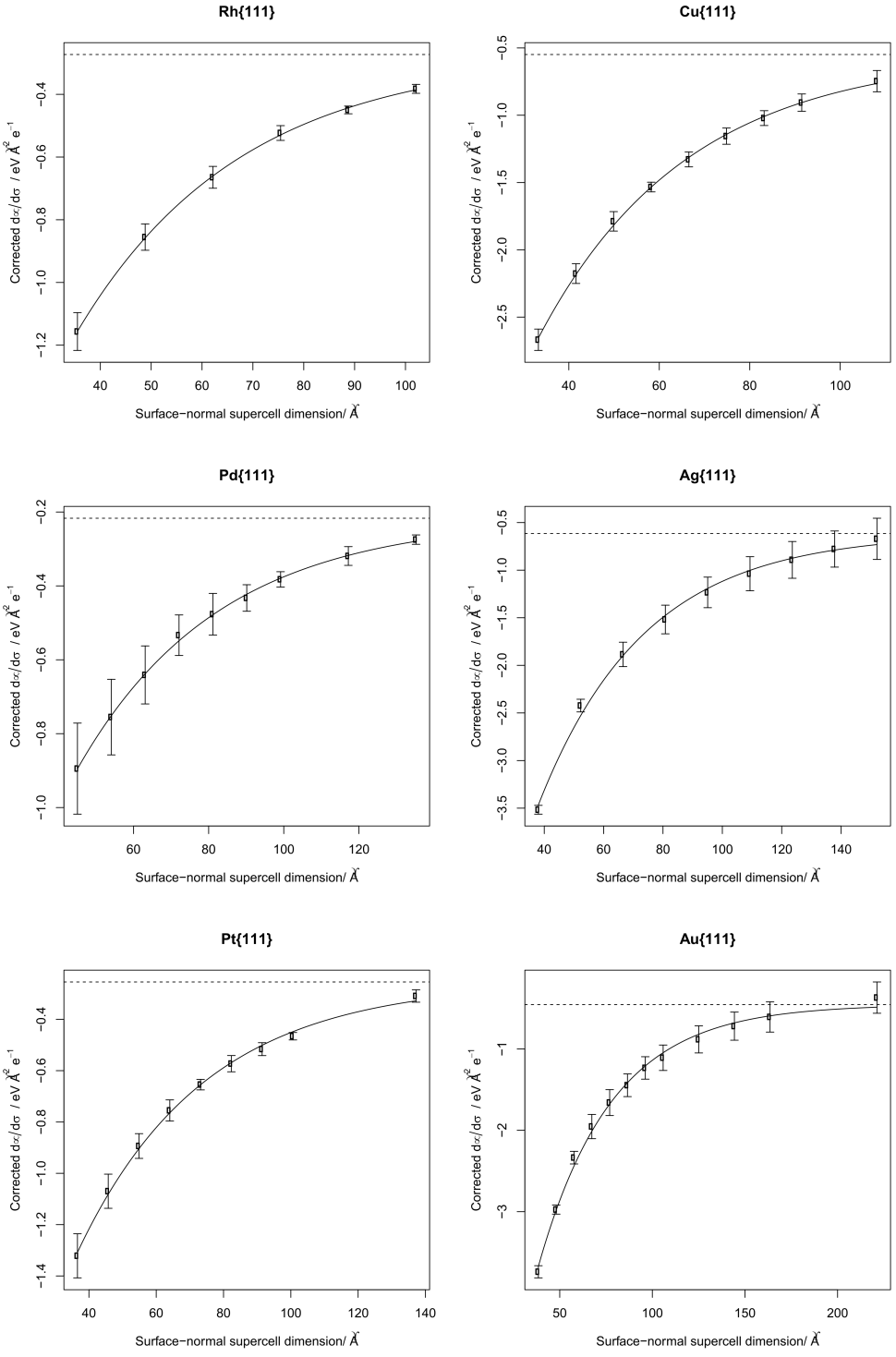

Figure S3: Comparison of denominator convergence for {111} surfaces of different metals. A constant 1:1 slab to vacuum ratio was used.

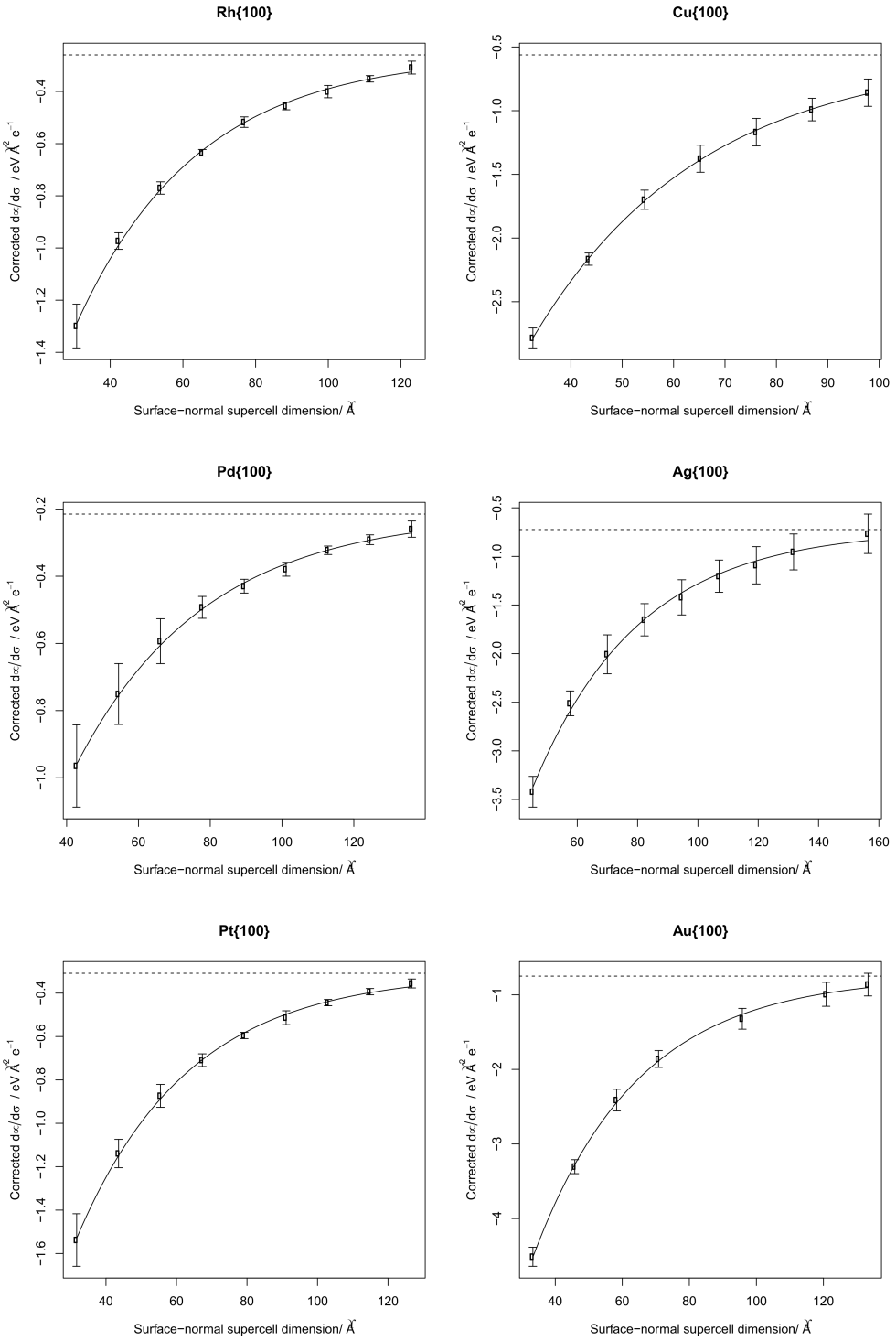

Figure S4: Comparison of denominator convergence for {100} surfaces of different metals. A constant 1:1 slab to vacuum ratio was used.

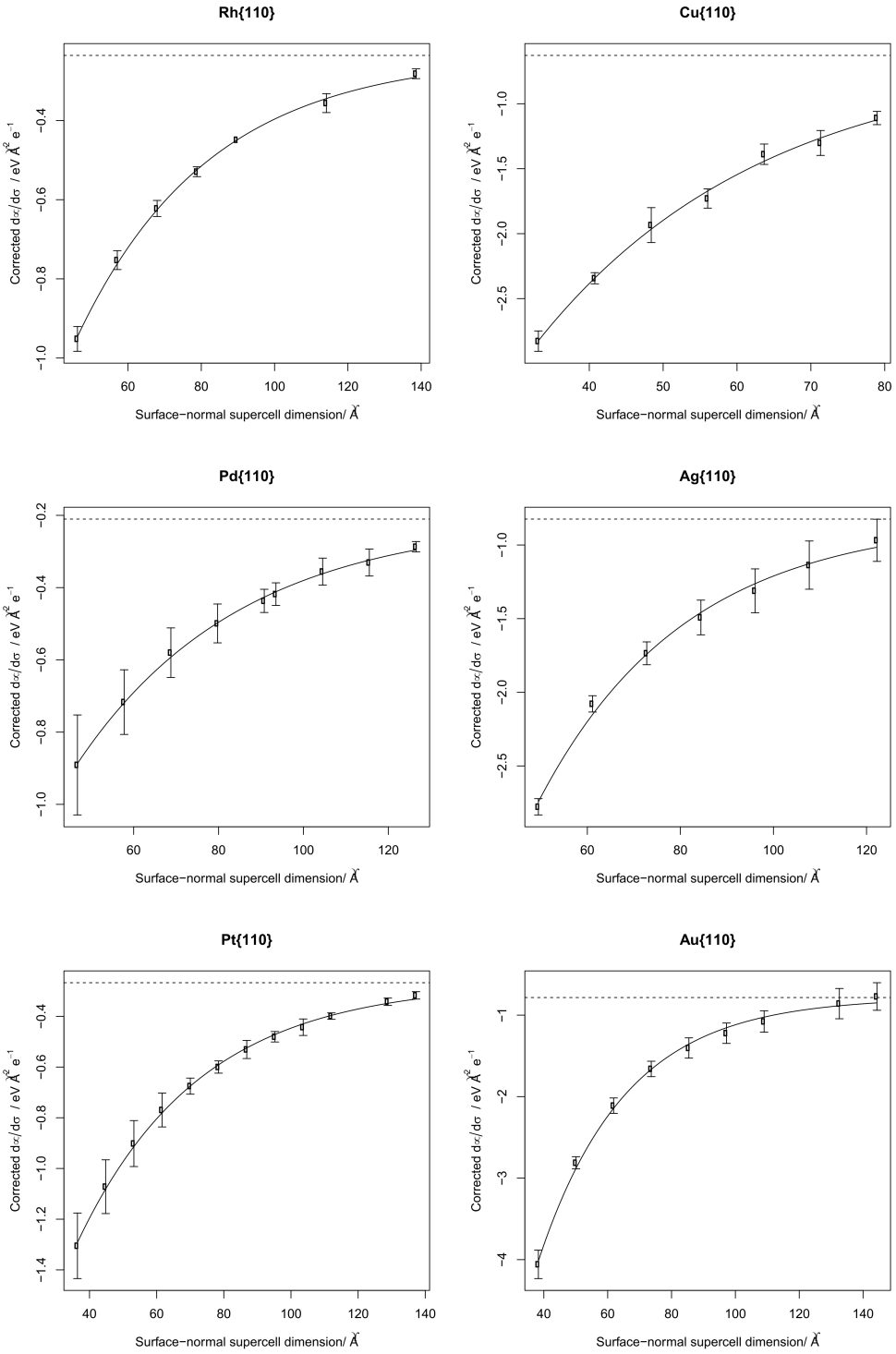

Figure S5: Comparison of denominator convergence for {110} surfaces of different metals. A constant 1:1 slab to vacuum ratio was used.

FITTING PARAMETERS FOR THE SOFTNESS DENOMINATOR

Fitting parameters of the exponentials from the preceding section are summarised in Table S6. The asymptotic value of the exponential, A, was taken as the standard denominator of local softness for each surface. The table shows a smaller magnitude of this parameter for the three transition metals compared with the coinage metals, implying an inherent tendency toward larger local softness.

Surface	A / eV Å^2 e^{-1}	B / eV Å^2 e^{-1}	k / Å^{-1}
Rh{111}	-0.273	-2.65	-0.0309
Rh{100}	-0.260	-2.58	-0.0299
Rh{110}	-0.235	-2.54	-0.0276
Pd{111}	-0.217	-2.24	-0.0265
Pd{100}	-0.215	-2.44	-0.0277
Pd{110}	-0.210	-2.28	-0.0259
Pt{111}	-0.254	-2.77	-0.0265
Pt{100}	-0.308	-3.30	-0.0314
Pt{110}	-0.267	-2.78	-0.0274
Cu{111}	-0.549	-5.80	-0.0305
Cu{100}	-0.562	-6.00	-0.0305
Cu{110}	-0.628	-6.43	-0.0324
Ag{111}	-0.615	-8.26	-0.0280
Ag{100}	-0.724	-9.62	-0.0285
Ag{110}	-0.824	-9.21	-0.0317
Au{111}	-0.456	-8.46	-0.0251
Au{100}	-0.748	-10.9	-0.0319
Au{110}	-0.784	-13.2	-0.0368

TABLE S6: Table of fitted parameters obtained by modelling the convergence of the denominator of local softness with an exponential of the form $A + B\exp(kc)$ where c is the supercell surface-normal dimension.

PLANAR-AVERGAED PLOTS OF LOCAL SOFTNESS

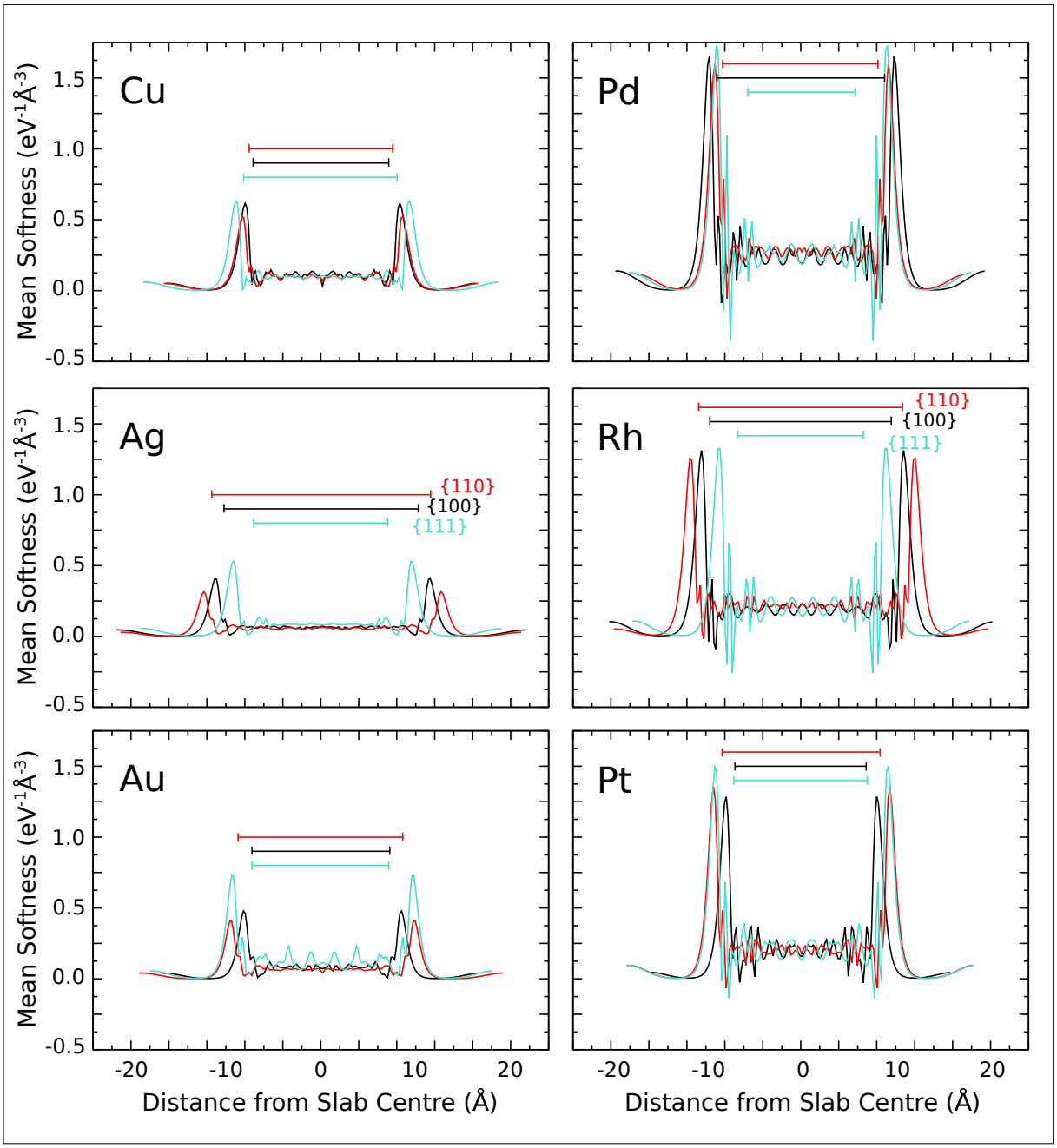

Figure S6: Planar-averaged softness values for all studied slabs as a function of distance from the slab centre. Black, blue, and red curves correspond to the 100, 111, and 110 surface orientations, respectively. Horizontal bars indicate the separation of the outermost layers of each slab, measured from the nuclear coordinates.

ISOSURFACES OF LOCAL SOFTNESS

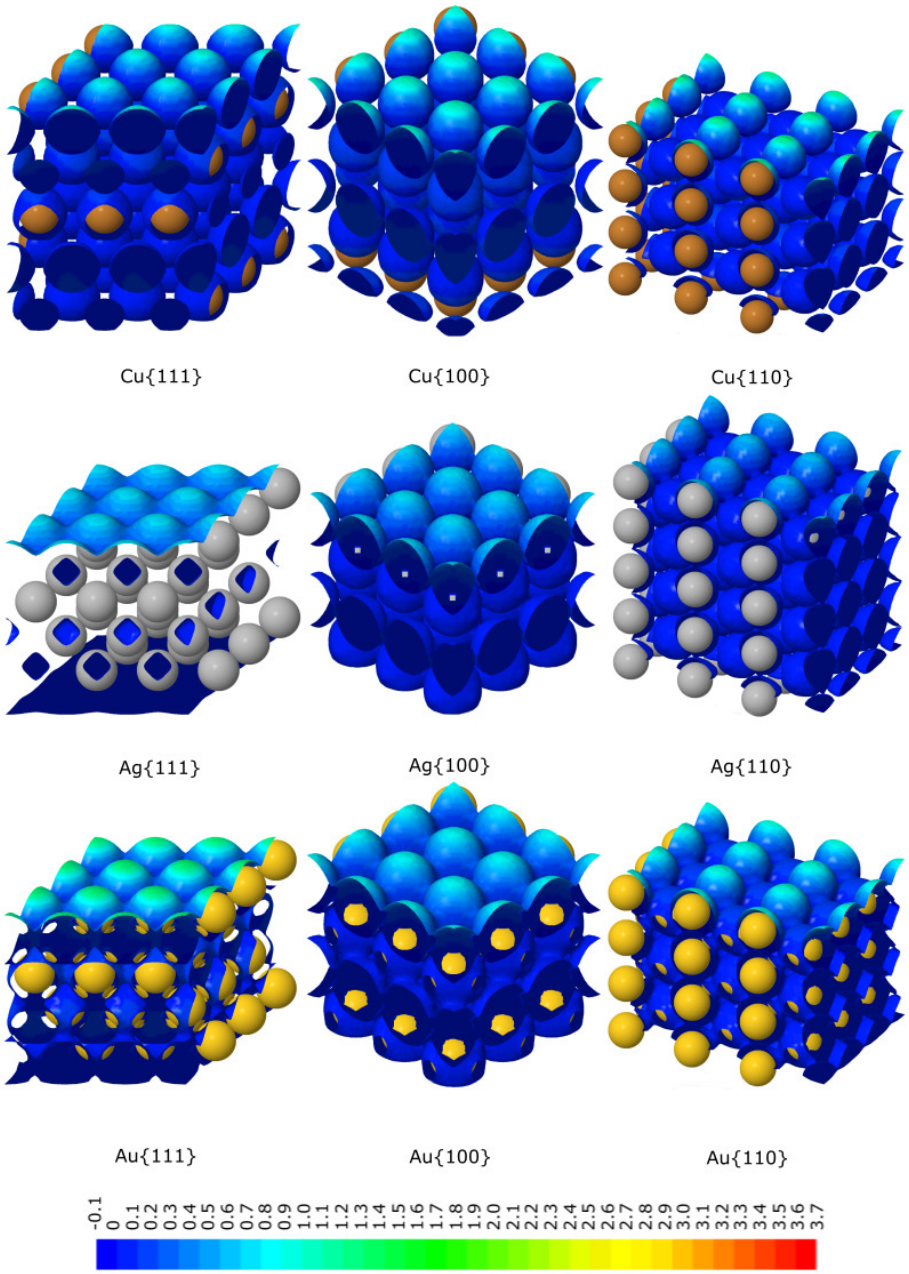

Figure S7: Side views of the local softness for all studied coinage metal surfaces, projected onto an isosurface corresponding to a valence electron density of one-third of its bulk value.

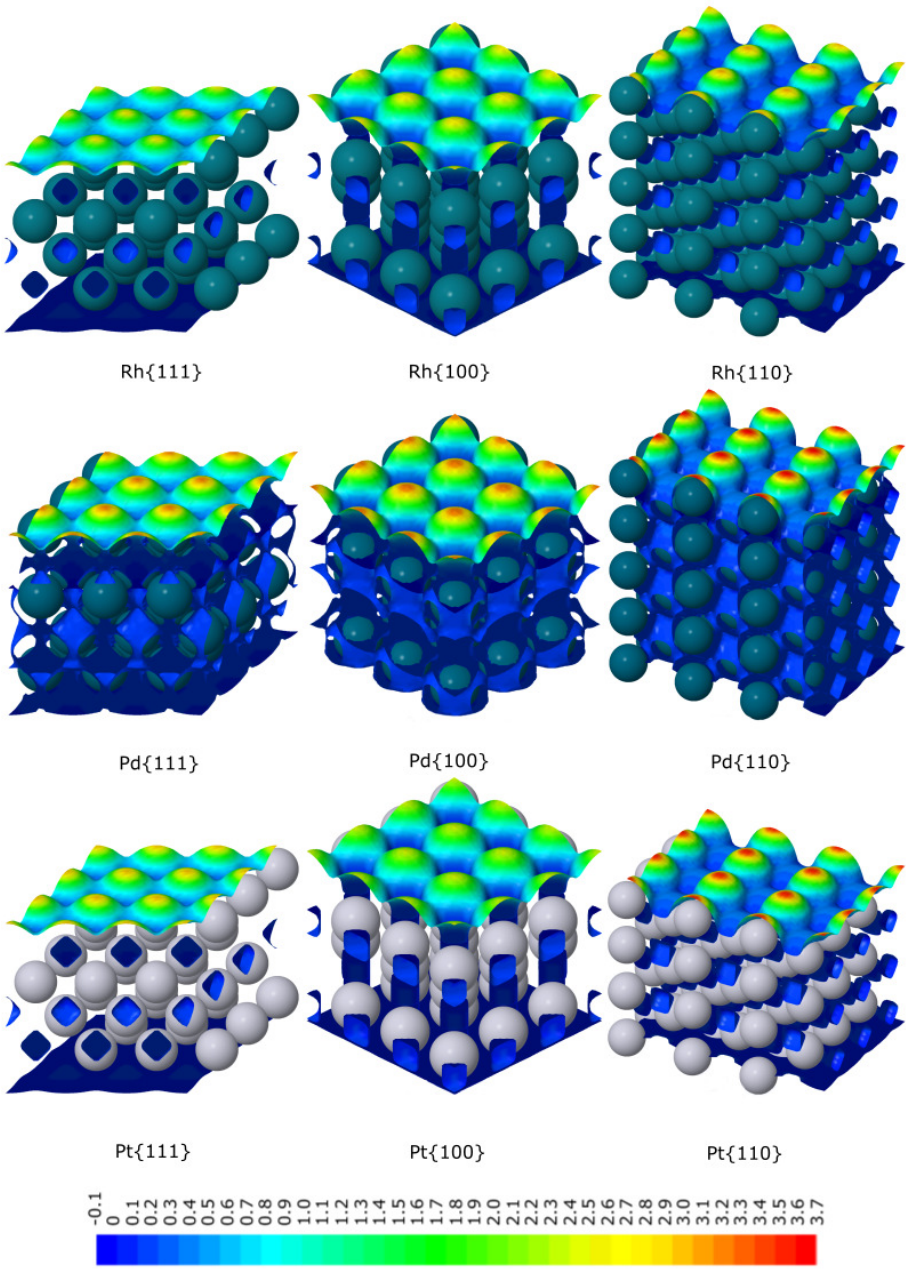

Figure S8: Side views of the local softness for all studied transition metal surfaces, projected onto an isosurface corresponding to a valence electron density of one-third of its bulk value.

TABLES OF ADSORPTION ENERGIES AND TOP-LAYER SOFTNESS VALUES

Surface	s_1 / eV^{-1}	CO Adsorption Energy/ eV	Coverage/ ML
Cu{111}	5.475	-1.099	1/3
Ag{100}	5.521	-0.548	1/2
Ag{110}	5.732	-0.625	1/2
Au{100}	6.280	-0.621	1/2
Cu{100}	6.344	-1.288	1/2
Ag{111}	6.626	-0.479	1/3
Cu{110}	6.941	-1.323	1/2
Au{110}	7.084	-0.843	1/2
Au{111}	8.740	-0.481	1/3
Rh{111}	12.988	-1.960	1/3
Rh{100}	14.276	-1.998	1/2
Pt{100}	14.798	-2.050	1/2
Pt{111}	14.969	-1.736	1/3
Pd{111}	16.896	-2.219	1/3
Pd{100}	18.388	-2.101	1/2
Rh{110}	18.870	-2.098	1/2
Pt{110}	20.002	-1.981	1
Pd{110}	24.129	-1.491	1

TABLE S7: Table showing the top-layer atomic softness, s_1, and calculated CO adsorption energy at the literature adsorption site for eighteen different metal surfaces. The adsorption energies are all for the most favourable site based on the experimental literature.

Surface	s_1 / eV^{-1}	CO Adsorption Energy/ eV	Coverage/ ML
Cu{111}	5.475	-1.099	1/3
Ag{100}	5.521	-0.548	1/2
Ag{110}	5.732	-0.625	1/2
Au{100}	6.280	-0.621	1/2
Cu{100}	6.344	-1.288	1/2
Ag{111}	6.626	-0.479	1/3
Cu{110}	6.941	-1.323	1/2
Au{110}	7.084	-0.843	1/2
Au{111}	8.740	-0.481	1/3
Rh{111}	12.988	-2.202 (-1.960)	1/3
Rh{100}	14.276	-2.282 (-1.998)	1/2
Pt{100}	14.798	-2.267 (-2.050)	1/2
Pt{111}	14.969	-1.954 (-1.736)	1/3
Pd{111}	16.896	-1.680 (-1.464)	1/3
Pd{100}	18.388	-1.771 (-1.568)	1/2
Rh{110}	18.870	-2.365 (-1.998)	1/2
Pt{110}	20.002	-2.409 (-2.201)	1/2
Pd{110}	24.129	-1.850 (-1.666)	1/2

TABLE S8: Table showing the top-layer atomic softness and calculated atop site CO adsorption energy for eighteen different metal surfaces. The adsorption energies are all for CO adsorption at the atop site, even where a different site would have a more exothermic adsorption. Also the coverages were kept at 0.5 ML or below, and the un-reconstructed surfaces were used, even where this was found not to be the case experimentally. Values in parentheses were calculated without dispersion correction.

[1] D. Wei, D. Skelton, and S. Kevan, Desorption and molecular interactions on surfaces: CO/Rh (110), CO/Rh (100) and CO/Rh (111), Surf. Sci. **381**, 49 (1997).

[2] R. Marbrow and R. Lambert, Chemisorption, Surface Structural Chemistry, and Electron-Impact Properties of Carbon-Monoxide on Rhodium (110), Surf. Sci. **67**, 489 (1977).

[3] J. Batteas, A. Barbieri, E. Starkey, M. Van Hove, and G. A. Somorjai, A tensor LEED analysis of the Rh(110)-p2mg(2 x 1)-2CO structure, Surf. Sci. **313**, 341 (1994).

[4] R. L. Park and H. H. Madden, Annealing changes on the (100) surface of palladium and their effect on CO adsorption, Surf. Sci. **11**, 188 (1968).

[5] R. J. Behm, K. Christmann, G. Ertl, M. A. Van Hove, P. A. Thiel, and W. H. Weinberg, The structure of CO adsorbed on Pd(100): A LEED and HREELS analysis, Surf. Sci. **88**, L59 (1979).

[6] R. Raval, S. Haq, M. Harrison, G. Blyholder, and D. King, Molecular Adsorbate-Induced Surface Reconstruction - CO/Pd(110), Chem. Phys. Lett. **167**, 391 (1990).

[7] R. J. Behm, P. A. Thiel, P. R. Norton, and G. Ertl, The interaction of CO and Pt(100). I. Mechanism of adsorption and Pt phase transition, J. Chem. Phys. **78**, 7437 (1983).

[8] P. A. Thiel, R. J. Behm, P. R. Norton, and G. Ertl, The interaction of CO and Pt(100). II. Energetic and kinetic parameters, J. Chem. Phys. **78**, 7448 (1983).

[9] C. M. Comrie and R. M. Lambert, Chemisorption and surface structural chemistry of carbon monoxide on Pt(110), J. Chem. Soc., Faraday trans. **72**, 1659 (1976).

[10] F. Abild-Pedersen and M. P. Andersson, CO adsorption energies on metals with correction for high coordination adsorption sites – A density functional study, Surf. Sci. **601**, 1747 (2007).

[11] G. McElhiney, H. Papp, and J. Pritchard, The adsorption of Xe and CO on Ag(111), Surf. Sci. **54**, 617 (1976).

[12] W. Hansen, M. Bertolo, and K. Jacobi, Physisorption of CO on Ag(111): Investigation of the monolayer and the multilayer through HREELS, ARUPS, and TDS, Surf. Sci. **253**, 1 (1991).

[13] U. Burghaus, L. Vattuone, P. Gambardella, and M. Rocca, HREELS study of CO oxidation on Ag(001) by O2 or O, Surf. Sci. **374**, 1 (1997).

[14] S. Krause, C. Mariani, K. C. Prince, and K. Horn, Screening effects in photoemission from weakly bound adsorbates: CO on Ag(110), Surf. Sci. **138**, 305 (1984).

[15] S. A. C. Carabineiro and B. E. Nieuwenhuys, Adsorption of small molecules on gold single crystal surfaces, Gold Bull. **42**, 288 (2009).

[16] L. Piccolo, D. Loffreda, F. Aires, C. Deranlot, Y. Jugnet, P. Sautet, and J. C. Bertolini, The adsorption of CO on Au(111) at elevated pressures studied by STM, RAIRS and DFT calculations, Surf. Sci. **566**, 995 (2004).

[17] M. S. Pierce, K.-C. Chang, D. C. Hennessy, V. Komanicky, A. Menzel, and H. You, CO-induced lifting of Au(001) surface reconstruction, J. Phys. Chem. C **112**, 2231 (2008).

[18] I. Nakamura, A. Takahashi, and T. Fujitani, Selective Dissociation of O-3 and Adsorption of CO on Various Au Single Crystal Surfaces, Catal. Lett. **129**, 400 (2009).

[19] Y. Jugnet, F. J. Cadete Santos Aires, C. Deranlot, L. Piccolo, and J. C. Bertolini, CO chemisorption on Au(110) investigated under elevated pressures by polarized reflection absorption infrared spectroscopy and scanning tunneling microscopy, Surf. Sci. **521**, L639 (2002).

[20] V. R. Dhanak, A. Baraldi, G. Comelli, G. Paolucci, M. Kiskinova, and R. Rosei, CO adsorption on unreconstructed and reconstructed Rh(110) surfaces: LEED and XPS studies, Surf. Sci. **295**, 287 (1993).

[21] A. Sandell, P. Bennich, A. Nilsson, B. Hernnas, O. Bjorneholm, and N. Martensson, Chemisorption of CO on Cu(100), Ag(110) and Au(110), Surf. Sci. **310**, 16 (1994).

[22] R. Meyer, C. Lemire, S. K. Shaikhutdinov, and H. Freund, Surface chemistry of catalysis by gold, Gold Bull. **37**, 72 (2004).

[23] J. M. Gottfried, K. J. Schmidt, S. L. M. Schroeder, and K. Christmann, Adsorption of carbon monoxide on Au(110)-(1 x 2), Surf. Sci. **536**, 206 (2003).

[24] K. F. Peters, P. Steadman, H. Isern, J. Alvarez, and S. Ferrer, Elevated-pressure chemical reactivity of carbon monoxide over Au(111), Surf. Sci. **467**, 10 (2000).

[25] R. Kose, W. A. Brown, and D. A. King, Role of lateral interaction in adsorption kinetics: CO/Rh{100}, J. Phys. Chem. B **103**, 8722 (1999).

[26] P. A. Thiel, E. D. Williams, J. T. Yates, and W. H. Weinberg, The chemisorption of CO on Rh(111), Surf. Sci. **84**, 54 (1979).

[27] Y. Y. Yeo, L. Vattuone, and D. A. King, Calorimetric investigation of NO and CO adsorption on Pd{100} and the influence of preadsorbed carbon, J. Chem. Phys. **106**, 1990 (1997).

[28] H. Conrad, G. Ertl, J. Koch, and E. E. Latta, Adsorption of CO on Pd single crystal surfaces, Surf. Sci. **43**, 462 (1974).

[29] J.-H. Fischer-Wolfarth, J. A. Farmer, J. M. Flores-Camacho, A. Genest, I. V. Yudanov, N. Rösch, C. T. Campbell, S. Schauermann, and H.-J. Freund, Particle-size dependent heats of adsorption of CO on supported Pd nanoparticles as measured with a single-crystal microcalorimeter, Phys. Rev. B **81**, 241416(R) (2010).

[30] Y. Y. Yeo, L. Vattuone, and D. A. King, Energetics and kinetics of CO and NO adsorption on Pt{100}: Restructuring and lateral interactions, J. Chem. Phys. **104**, 3810 (1996).

[31] C. E. Wartnaby, A. Stuck, Y. Y. Yeo, and D. A. King, Microcalorimetric heats of adsorption for CO, NO, and oxygen on Pt{110}, J. Phys. Chem. **100**, 12483 (1996).

[32] Y. Y. Yeo, L. Vattuone, and D. A. King, Calorimetric heats for CO and oxygen adsorption and for the catalytic CO oxidation reaction of Pt{111}, J. Chem. Phys. **106**, 392 (1997).
[33] E. Haynes, W. M., *CRC Handbook of Chemistry and Physics* (CRC Press, 2014).
[34] G. Kresse and D. Joubert, From ultrasoft pseudopotentials to the projector augmented-wave method, Phys. Rev. B **59**, 1758 (1999).